Journal of Inorganic and Organometallic Polymers and Materials
https://doi.org/10.1007/s10904-026-04318-5

RESEARCH

Eco-friendly Synthesis and Characterization of ZnO and CdS Nanoparticles Using *Rhus coriaria* Extract for Antibacterial and Antifungal Applications

Samir Mustafa Hamad[1] · Renjbar Muksy Mhamedsharif[1] · Parwin Jalal Jalil[1] · Dlgash Hamad Maruf[1] · Peyman Aspoukeh[1] · Dilshad Shaikhah[1,2]

Received: 24 March 2026 / Accepted: 21 April 2026
© The Author(s) 2026

Abstract

This study involved the preparation of ZnO and CdS nanoparticles via a plant-assisted aqueous synthesis method using *Rhus coriaria* extract, followed by assessment of their structural, optical, and antibacterial properties. We used X-ray diffraction (XRD), UV–Vis spectroscopy, Fourier-transform infrared spectroscopy (FTIR), scanning electron microscopy (SEM), and energy-dispersive spectroscopy (EDS) to study the nanoparticles we made. The XRD showed that crystalline hexagonal ZnO and CdS phases had formed. The average diameters of the crystals were about 31.2 nm and 41.28 nm, respectively. The UV–Vis investigation showed that ZnO had an absorption band at 370 nm and CdS had an absorption band at 463 nm. These bands correspond to band-gap energies of 3.29 eV and 2.72 eV, respectively. SEM showed that ZnO particles were grouped together and were about 71.9 nm in size, while CdS particles were about 83.39 nm in size. FTIR spectra showed the presence of hydroxyl and organic surface groups, suggesting that plant-based compounds helped stabilize the nanoparticles. Antimicrobial testing showed that both nanoparticles were effective against *Klebsiella pneumoniae* (22.2 ± 0.6 and 32.1 ± 1.05) mm and *Staphylococcus aureus* (23.4 ± 0.3 and 33.2 ± 0.6) mm for ZnO and CdS NPs, respectively at 100 mg/mL, although CdS was more effective overall and was the only material that worked against *Candida albicans* (29.0 ± 1.2) mm. Under the conditions tested, ZnO did not exhibit any antifungal activity. These results show that using *Rhus coriaria* to produce ZnO and CdS nanoparticles is an effective method, but further research on the mechanisms, surface properties, yield optimization, and toxicity is needed before it can be used in real life.

Keywords Antibacterial · Antifungal · CdS NPs · Green Synthesis · ZnO NPs

1 Introduction

Nanoparticles (NPs) with dimensions ranging from 1–100 nm play important roles in various fields [1]. Nanotechnology is a cutting-edge subject to investigate that is gaining extensive attention and is important to pharmacology and medicine. It has become one of the developing multidisciplinary fields [2]. These nanomaterials exhibit a significantly higher surface area-to-volume ratio and can show improved of magnetic, electrical, optical, mechanical, and catalytic properties [3]. NPs are currently the target of extensive scientific research due to their potential uses in a variety of areas including research medical studies, waste water treatment, drug delivery, agriculture, and sensor [4–8].

Nowadays, different technologies, including chemical, physical, and biological approaches, are used for the synthesis of nanomaterials [9]. Physical methods are typically defined by the need of high vacuum and high temperatures, together with the use of advanced equipment [10]. In contrast, chemical methods involve considerable environmental and health hazards owing to the use of toxic compounds as reducing and capping agents [11]. In recent years, there has been a significant shift towards biological methods in

✉ Dilshad Shaikhah
d.m.shaikhah@leeds.ac.uk

[1] Scientific Research Centre, Soran University, Soran 44008, Kurdistan Region, Iraq

[2] Institute of Functional Surfaces, School of Mechanical Engineering, University of Leeds, Leeds LS2 9JT, UK

Published online: 17 June 2026

the formation of metal and metal oxide NPs, mostly due to their reduced environmental impact. These approaches employ different biogenic materials, including bacteria, fungui, yeast, and plant-derived components, including leaves, fruits, and vegetables, which function as bioreactors for NPs synthesis [12]. The synthesis of NPs from plants is considered a sustainable and green option, providing significant benefits, especially in biomedical sciences and applications. Plant extracts are increasingly valued for their abundant phytochemicals, including flavonoids, glycosides, polyphenols, terpenoids, and enzymes, which serve crucial functions as reducing, capping, and stabilizing agents [13–15]. *Rhus coriaria L.* (*R. coriaria*) plant is a member of the Anacardiaceae family, generally known as sumac, and has been widely consumed as a traditional condiment and herbal remedy throughout the Mediterranean for decades [16]. *R. coriaria* has gained popularity in recent years due to its medicinal properties. Sumac has many health benefits due to its phytochemical compounds, such as phenolic acids, flavonoids, and tannins [17], including anticancer, antioxidant, antimicrobial, anti-inflammatory, antifungal, hypoglycemic, hypolipidemic, neuroprotective, and anti-atherogenic properties [18]. Also the plants rich in phytochemical content function as natural reducing and stabilizing agents for NPs synthesize. These compounds promote the conversion of metal salt precursors into NPs without the need for toxic chemical reagents.

The morphological characteristics, such as shape and size, of NPs are essential in controlling the mechanical, electrical, and optical properties of the produced nanomaterials [19]. It is essential to highlight the main differences between biosynthesis and other NPs creation techniques. In biosynthesis, the reduction and stability of NPs are mostly facilitated by phytochemicals present in plant extracts. These phytochemicals are distinguished by their non-toxicity, cost-effectiveness, and environmental sustainability, and the synthesis process generally occurs in a single reaction vessel [20, 21].

Nanomaterials have attracted considerable interest in their antibacterial activities. A wide range of NPs, such as iron oxide, copper oxide, titanium dioxide, zinc oxide, magnesium oxide, silica, and silver, have exhibited antibacterial properties [22–24]. ZnO and CdS NPs are distinguished among different nanomaterials for their exceptional physicochemical features and promising biological activity, particularly their antimicrobial (antibacterial and antifungal) capabilities [25–27]. Both NPs are recognized for their antibacterial properties owing to their cost-effectiveness, biocompatibility, and high surface area-to-volume ratio, which improves interaction with microorganisms. They demonstrate broad activity against many bacterial and fungal infections, including both Gram-positive and Gram-negative microorganisms. Their antibacterial properties mostly arise from the generation of reactive oxygen species (ROS), which induce oxidative stress and harm cellular structures, alongside the release of ions that damage cell membranes and affect metabolic processes [28]. ZnO NPs are beneficial against fungus, probably through damaging fungal cell membranes and influencing their metabolic pathways. While CdS NPs exhibit activity against many bacterial strains and fungal pathogens, their use is more limited than that of ZnO due to concerns over cadmium toxicity. Researchers are developing techniques to functionalize or encapsulate CdS NPs to reduce toxicity while maintaining antibacterial efficiency. CdS NPs have potential applications in antifungal treatments, antibacterial coatings, and water treatment systems for the control of microbial contamination [29, 30]. Although antibiotics are the principal treatment, microbial resistance, enhanced by inefficient drug usage and environmental spread of antibiotics, poses a considerable concern [31]. NPs-based therapies, potentially utilized with antibiotics, present a promising approach to reduce resistance and improve therapeutic effectiveness [32]. These NPs efficiently inhibit biofilm formation, a critical resistance mechanism of bacteria and fungi, hence eliciting bactericidal and fungicidal effects [33]. Comparable antibiofilm effects were noted using TiO2 NPs against fungal biofilms (Antifungal Activity of TiO_2 NPs and EDTA on *Candida albicans* (*C. albicans*) Biofilms. Sharma et al. studied the chemically synthesized ZnO NPs with and without surfactants under varied reaction conditions, the size of NPs ranged from 2 to 28 nm in diameter. They showed promising particle size-dependent antibacterial and antifungal properties.

Kakanejadifard, Khojasteh [34] investigated the Ag and CdS NPs that were produced utilizing an azo-Schiff base ligand (L) as both capping and reducing agent and tested for antibacterial activity against diverse bacterial and fungal species. Antibacterial activity of the azo-Schiff base ligand was limited to Gram-positive *Bacillus cereus*. In contrast, L-capped Ag-NPs showed moderate to strong antibacterial activity against Gram-positive and Gram-negative bacteria. Additionally, L-capped CdS-NPs inhibited Gram-positive and Gram-negative bacteria *B. cereus* and *Escherichia coli (E.coli)*. All chemicals inhibited fungal strains. The process by which NPs inhibit microorganisms is understood. The formation of insoluble compounds due to the inactivation of sulfhydryl groups on the target cell wall, along with the degradation of membrane-associated lipids and enzymes, may be the expected cause [35].

The nucleation rate, crystal development, agglomeration behavior, and final physicochemical properties of green NPs depend on reaction parameters like pH, temperature, precursor concentration, plant extract dose, and reaction

time. Ionization of phytochemicals and hydrolysis of metal precursors are particularly affected by pH. Temperature impacts crystal growth and reaction speed. Precursor/extract concentration regulates supersaturation and particle growth. The reaction length determines nanoparticle number and stability. To get consistent ZnO and CdS NPs, control these parameters.

This study aims to use a green method for fabricating ZnO and CdS NPs utilizing *Rhus coriaria* extract, then investigate their structural, optical, and antimicrobial properties. The synthesized NPs are evaluated for antibacterial and antifungal activity to develop biocompatible materials suitable for biomedical applications. To the best of our knowledge, no previous study has described the green synthesis of both ZnO and CdS NPs using *R. coriaria* extract, and the antibacterial activity of R. coriaria-derived CdS NPs has not been investigated. By comparing the efficacy of ZnO and CdS NPs, this research seeks to highlight the potential of *R. coriaria* as a versatile agent for the green synthesis of NPs, contributing to the growing field of green nanotechnology.

2 Materials and Methods

2.1 Chemicals and Materials

Zinc nitrate hexahydrate [$Zn(NO_3)_2.6H_2O$] and sodium hydroxide (NaOH) were supplied by Biochem, Cadmium acetate dihydrate [$Cd(CH_3COO)_2.2H_2O$] was acquired from SDFCL companies, and sodium sulfide (Na_2S) was attained from CDH company.

2.2 Plant Collection and Extractions

The *R. coriaria* were collected in Rowanduz City/Kurdistan Region-Iraq. Five gm of dried *R. coriaria* combined with 100 mL of double-distilled water, heated to 70 °C, and stirred for an hour. After cooling to room temperature, the mixture was filtered using filter paper. The extract was used immediately to create NPs (Fig. 1).

2.3 Green Synthesis of ZnO, and CdS Nanoparticles

Zinc nitrate $Zn(NO_3)_2.6H_2O$ (0.1 M) solution was prepared with vigorous heating and stirring at 80 °C for 15 min. A volume of 50 mL of *R. coriaria* extract was gradually 50 mL of a 1.43 g zinc nitrate solution, which was heated and stirred continuously. The pH of the solution was adjusted to approximately 11 by the addition of 1 M NaOH (2 g in 50 mL), resulting in a color transition of the mixture to light yellow and the initiation of precipitation. Following one hour of continued heating and stirring, the mixture was allowed to stand at room temperature overnight. The resultant precipitate was subsequently exposed to drying at 80 °C, followed by calcination at 500 °C for a duration of 1 h, leading to the formation of ZnO NPs. The synthesized ZnO NPs were cleaned twice with double-distilled water and once with ethanol and then dried in an oven at 80 °C to obtain pure ZnO NPs, as depicted in Fig. 2.

As revealed in Fig. 3, initially, 30 mL of plant extract was mixed with 1.01 gm (0.1 M) dissolved in 50 mL of double-distilled water of cadmium acetate dihydrate $Cd(O_2CCH_3)_2(H_2O)_2$ as a precursor solution, heated to 80 °C for 10 min, and stirred. Next, a yellow precipitate was generated when 0.39 gm in 50 mL of double-distilled water of (0.1 M) sodium sulfideNa_2S solution was added to the mixture dropwise. The mixture was stirred for an hour at 80 °C, allowed to settle overnight, and then cleaned with ethanol and

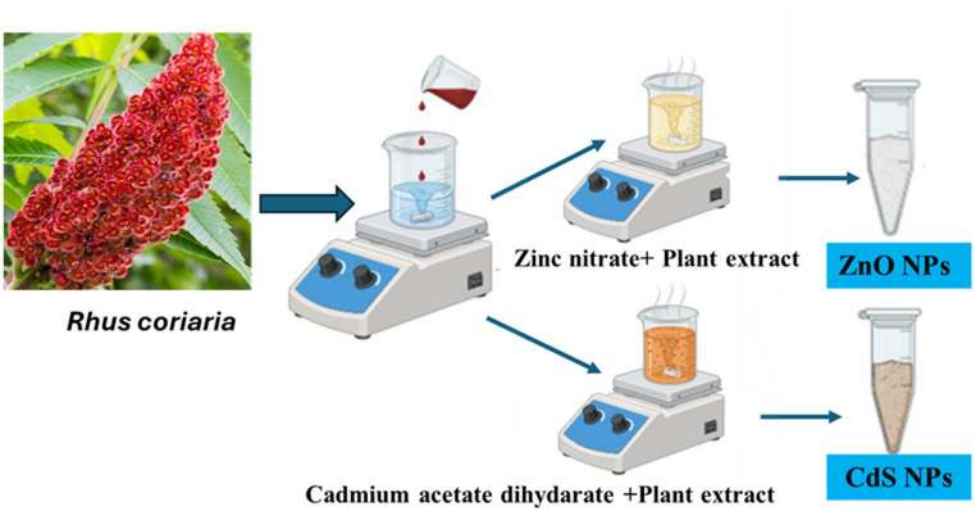


Fig. 1 Extraction of ZnO and CdS nanoparticles using *Rhus coriaria* extract.

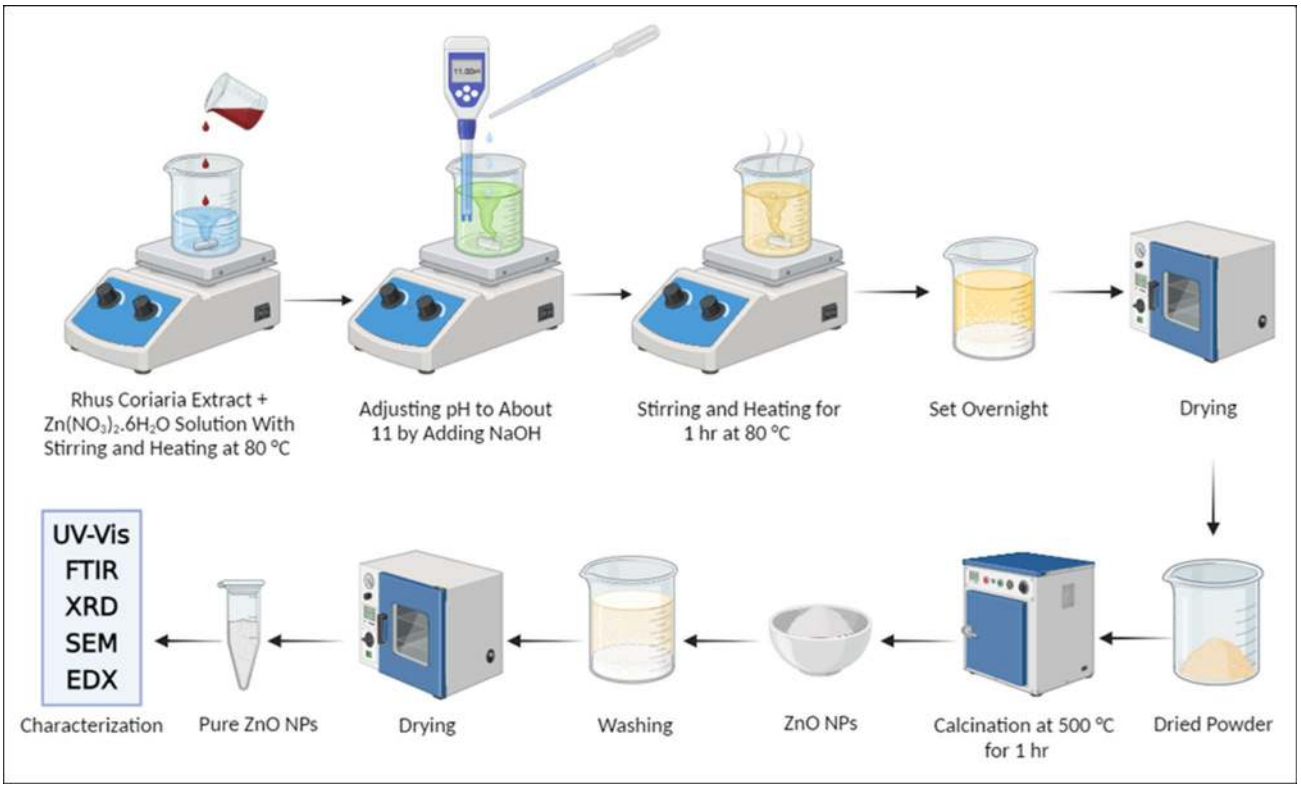


Fig. 2 Schematic illustration for the green synthesis of ZnO NPs

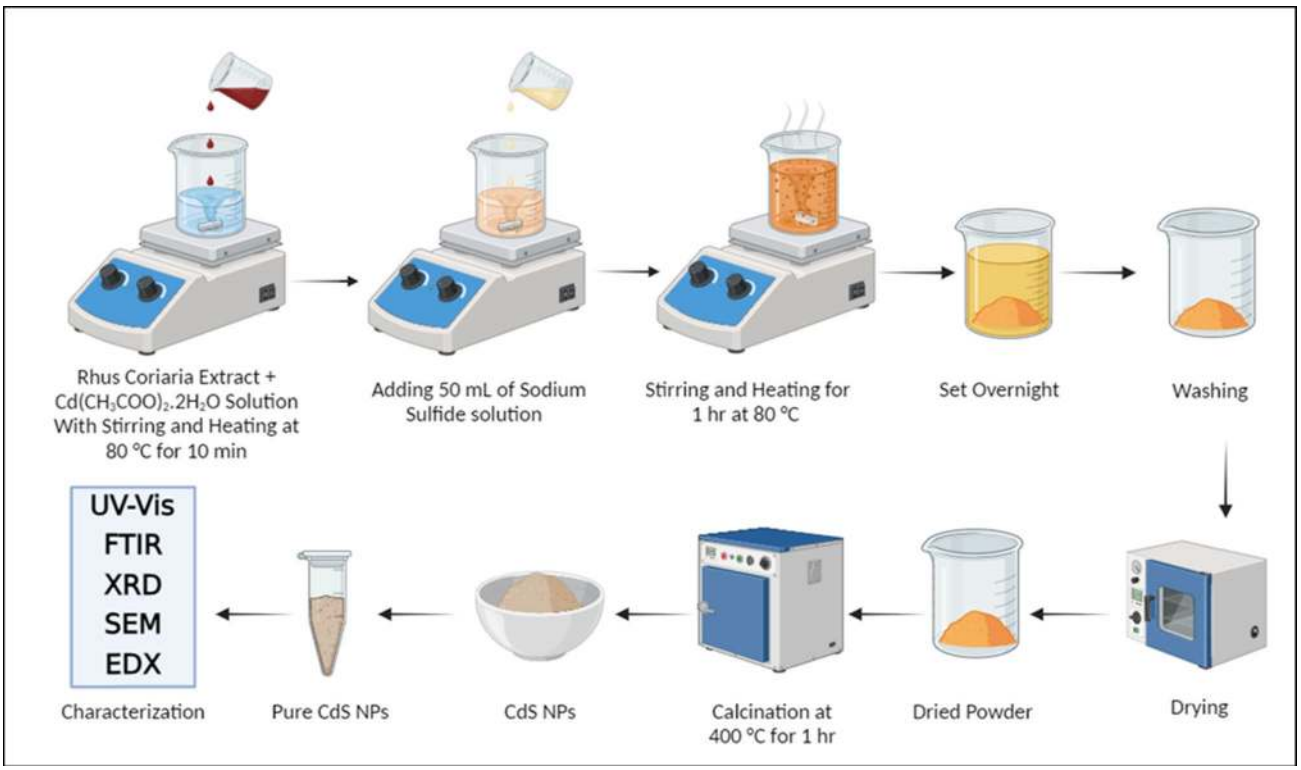


Fig. 3 Schematic illustration for the green synthesis of CdS NPs

double-distilled water. For one hour, the dry precipitate was calcined at 400 °C. Ultimately, CdS NPs were produced.

2.4 Characterizations of Synthesized ZnO NPs and CdS NPs

The formation of ZnO and CdS NPs was observed using a UV–Vis double-beam spectrophotometer (Super Aquarius-1000). The biomolecules from leaf extracts, which were attached to the NPs as a reducing and capping agent, were studied using a Fourier transform infrared (FTIR; Perkin Elmer) spectrophotometer over the range 400–4000 cm^{-1}. The structure of NPs was investigated using an X-ray diffraction (XRD) instrument from PANalytical (CuKα = 1.54 nm); the scan rate was 1°/min, ranging from 20° to 80°. Additionally, scanning electron microscopy (SEM-Quanta 450) was used to examine the morphology of the synthesized NPs. Also, by using energy-dispersive X-ray (EDX), the nanostructures' chemical composition was determined.

2.5 Antibacterial and Antifungal Activities of ZnO NPs and CdS NPs

To examine the effect of ZnO and CdS NPs on the growth of bacteria and their bactericidal activity, the Gram-negative bacteria (*Klebsiella pneumoniae and Pseudomonas aeruginosa*) and the Gram-positive bacterium (*Staphylococcus aureus*) were tested. The bacterial culture was activated in 100 mL of NB and incubated for 18 h at 37 °C. The bacteria were spread on sterile Muller-Hinton agar plates by using a sterile cotton swab and left for 10 min. Five concentrations were prepared from the NPs (2.5, 5, 7.5, 10, and 100 mg/mL) that were sonicated before use to test the nanoparticles NPs, and sterilized distilled water was used as a negative control. The broad antibacterial disc of the chloramphenicol and amoxicillin was used as a positive control. The well diffusion method was performed to test the NPs against the pathogenic bacteria by boring 5 wells in the cultured MHA media for each concentration of the NPs as prepared previously. All the plates were incubated at 37 °C for 24 h. The zone around the well was measured using a ruler. The antibacterial test was done in triplicate.

Antifungal activity of the synthesized ZnO and CdS NPs was evaluated against Candida *albicans by the well diffusion method using* MHA medium. Four concentrations were prepared from the (NPs; 2.55 mg/mL, 5 mg/mL, 7.55 mg/mL, 100 mg/mL, and 100 mg/mL), and sterilized distilled water was used as a negative control. Fluconazole and miconazole discs were used as positive control. All the plates were incubated at 37 °C for 24 h. The zone around the well was measured by using a ruler. The antifungal test was done in triplicate.

2.6 Statistical Analysis

All experimental data were expressed as mean ± standard error (SE). Statistical analysis was performed using one-way analysis of variance (ANOVA) to evaluate the significant differences among the means of different bacterial species treated with CdS NPs and ZnO NPs. When significant differences were detected, comparisons between groups were considered statistically significant at $p < 0.05$. All analyses were carried out using appropriate statistical software.

3 Results and Discussions

3.1 Characterization of Synthesized ZnO and CdS NPs from *Rhus coriora* Plant

3.1.1 UV- Vis Spectroscopy

The optical properties of ZnO NPs were examined using a UV–Vis spectrophotometer, a standard method employed for validating the synthesis of ZnO NPs. Figure 4 (A) presents the UV–Vis spectra obtained for the synthesized ZnO NPs. A distinct absorption band centered at 370 nm corroborates the presence of ZnO NPs within the solution. Notably, the UV–Vis analysis revealed the absence of additional absorption peaks, indicating the purity of the ZnO NPs. Furthermore, the obtained results exhibit excellent consistency with findings from prior studies [36].

The determination of the band gap energy was conducted using a Tauc plot, employing the following formula:

$$\alpha hv = A\,(hv - E_g)^n \tag{1}$$

In this methodology, where α represents the optical absorption parameter, hv denotes the energy of a photon, E_g signifies the direct band-gap, A stands for a constant, and the power n is contingent upon the nature of the optical transition. The process involves plotting $(\alpha hv)^n$ against hv, then extrapolating in the linear region along the energy axis in the associated graph. The direct band-gap is determined to be 3.29 eV for ZnO NPs, as depicted in Fig. 4 (A).

The fabrication of CdS NPs was characterized using a UV–Visible spectrophotometer. The absorbance spectrum was measured over 450–520 nm, revealing a strong absorption peak at 463 nm. The broad peaks observed suggest variability in the nanoparticle sizes. Additionally, the

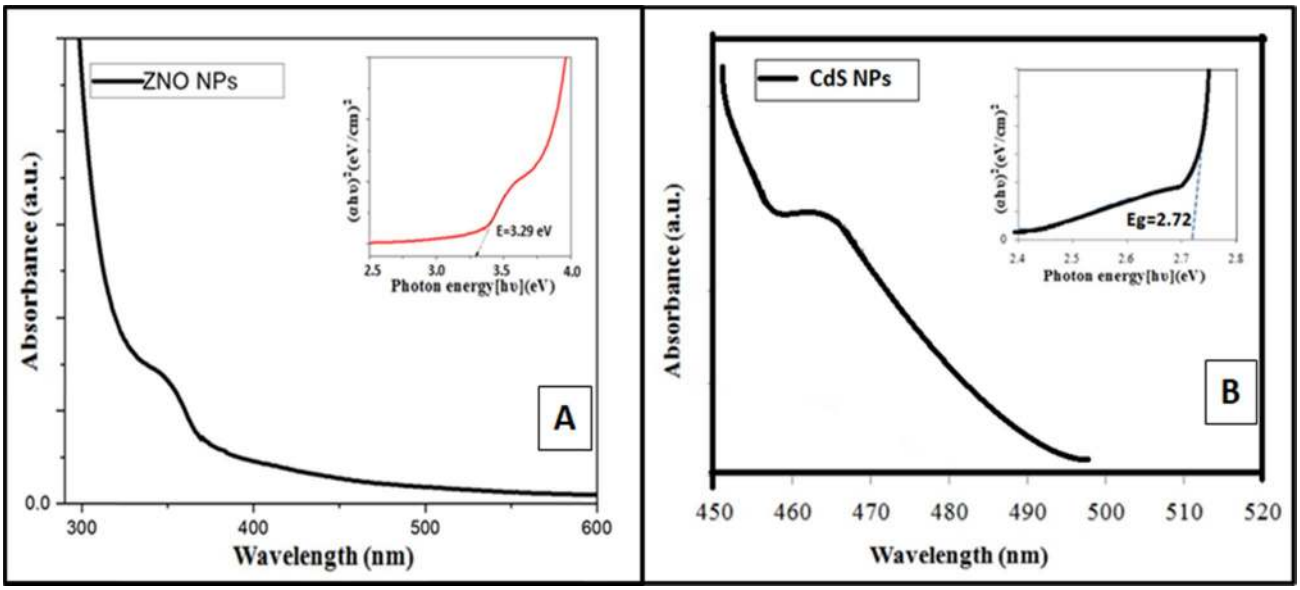


Fig. 4 UV–VIS absorption spectrum of **A** ZnO NPs and **B** CdS NPs

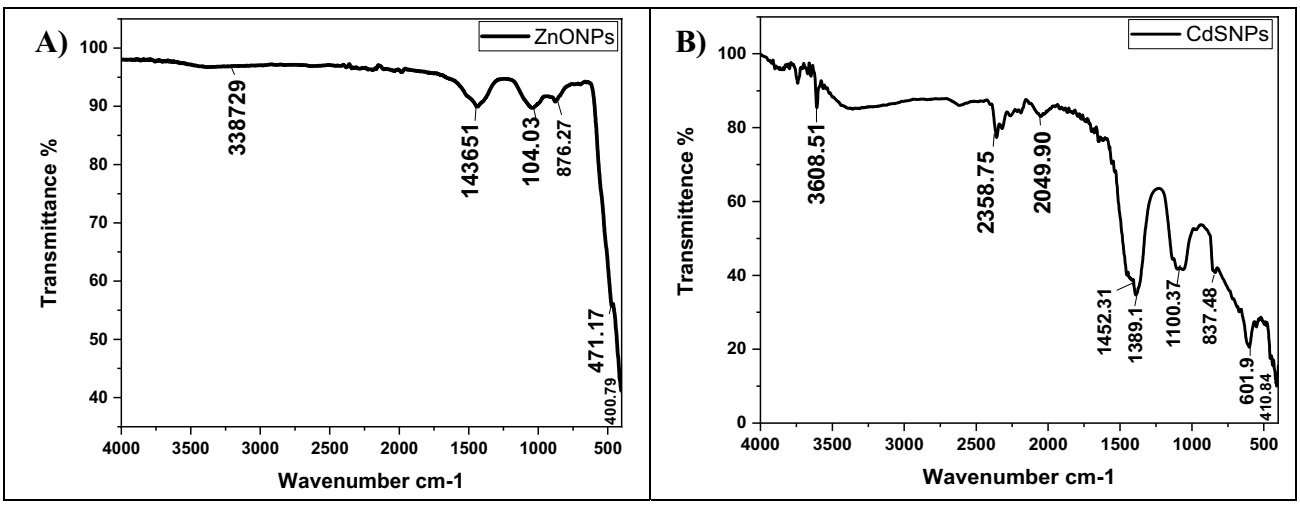


Fig. 5 The FTIR analysis of **A** ZnO NPs and **B** CdS NPs

direct band gap energy of the CdS NPs was determined to be 2.72 eV using a Tauc plot method. This information is typically depicted graphically, likely shown in the inset of Fig. 4 (B). The Tauc plot is commonly used to estimate the band gap energy of semiconductor materials based on their absorption spectra. The results show in good agreement with previous study findings [36].

3.1.2 FTIR Spectroscopy Analysis

The FTIR spectra of ZnO NPs within the wavenumber range of 400–4000 cm^{-1} are presented in Fig. 5 (A). Different characteristic peaks are observed at approximately 471, 876.27, 1004.03, 1436.56, and 3387.9 cm^{-1}. The FTIR analysis revealed broad and small absorption bands around 3400 cm^{-1}, attributed to the stretching vibration of the hydroxyl bonds (O–H) present on the surface of the NPs, as reported by Richter, Wang [37]This confirms the presence of water molecules adsorbed onto the nanoparticle's surface. Moreover, bands at 1436, 1004, and 876 cm^{-1} correspond to C-H stretching, C=O stretching, and C-H bending, respectively. The expression of betaine molecules serves as both a reducing and a capping agent on the surface of produced ZnO NPs, as considered in the previous work [38]. Also, bands at 471 and 400 cm^{-1} are attributed to the asymmetric stretching and bending vibrations of the Zn–O tetrahedron structure.

Consequently, Fig. 5 (B) displays the FTIR spectrum of green-synthesized CdS NPs, covering a wavelength range from 4,000 to 500 cm^{-1}. The broad peak at 3500 cm^{-1}

indicates the presence of hydroxyl groups within the structure. Bands detected around 2358 cm^{-1} are indicative of C-H interactions, while a distinct band at 1100 cm^{-1} suggests C-N vibrations, likely originating from aliphatic amines. Signals located near 1452 and 1389 cm^{-1} signify vibrations associated with C=O and N–H functional groups, characteristic of amines and amides [39]. Additionally, peaks observed at 2049 and 837 cm^{-1} may indicate the presence of C=C double bonds, potentially arising from either a ring structure or an aliphatic hydrocarbon chain. These biomolecules are supposed to be peptides or proteins, which likely play roles in both the nucleation process and the stabilization of NPs. It is reasonable that enzymes located on the cell membrane or suppressed into the extracellular background may contribute to the synthesis of NPs, as proposed by Hosseini and Sarvi [40]. Significant peaks relating to the Cd-S bond stretching mode are located in the fingerprint region of the spectra peaks at 601 and 570 cm^{-1} [41].

3.1.3 X-Ray Diffraction Study

Figure 6 (A) displays the XRD pattern from green synthesis ZnO NPs, scanned between 10 and 80 2theta degrees. This pattern confirmed the crystallin structure of produced ZnO nanostructures The (100), (002), (101), (012), (110), (013), (112), (201), (004), and (202) planes can be assigned to the 2θ peaks at 31.76°, 34.39°, 36.24°, 47.51°, 56.59°, 62.81°, 67.92°, 69.07°, 72.49°, and 76.94°, respectively. The results show that all diffraction peaks are indexed to the hexagonal wurtzite structure of ZnO NPs (ICSD Card no. 98-018-0051). These peaks are in complete agreement with earlier investigations [42]. Conversely, the XRD patterns of the prepared CdS NPs using plant extract are depicted in Fig. 6 (B). The diffraction peaks at 2θ = 24.8, 26.5, 28.1, 36.6, 43.6, 47.8 and 51.8 can be indexed to the planes (100), (002), (101), (102), (110), (103) and (112) of hexagonal crystal structure CdS NPs respectively, (ICDD PDF 89-0440) [43]. The narrow and high intensity of diffraction peaks indicated that the NPs have a high-quality structure.

Furthermore, the XRD patterns of ZnO and CdS NPs reveal no extra peak, indicating that pure green synthesis nanomaterials were utilized. The size of the fabricated crystallites, ZnO and CdS NPs, was determined using the Debye–Scherrer formula:

$$D = 0.95\lambda / (\beta \cos\theta) \quad (2)$$

Where D is the average crystallite size, λ is the wavelength of the incident X-ray (0.154 nm), θ is Bragg'sangle, and β is the full width at half maximum (FWHM). Debye–Scherrer's equation is an approximate principle suitable only for spherical and semispherical particles [44]. From the above equation, the average crystallite size for ZnO NPs is measured to be ~ 31.2 nm, and for CdS NPs was 41.28 nm.

The comparative characterization in Table 1 shows that although both materials were made using the same plant-assisted method, they have different crystallite sizes, optical responses, and surface chemistry. This could explain why they have different antibacterial properties.

3.1.4 Morphological and Elemental Composition Study

The surface morphology of biosynthesized ZnO NPs was mainly characterized through FE-SEM analysis; the results

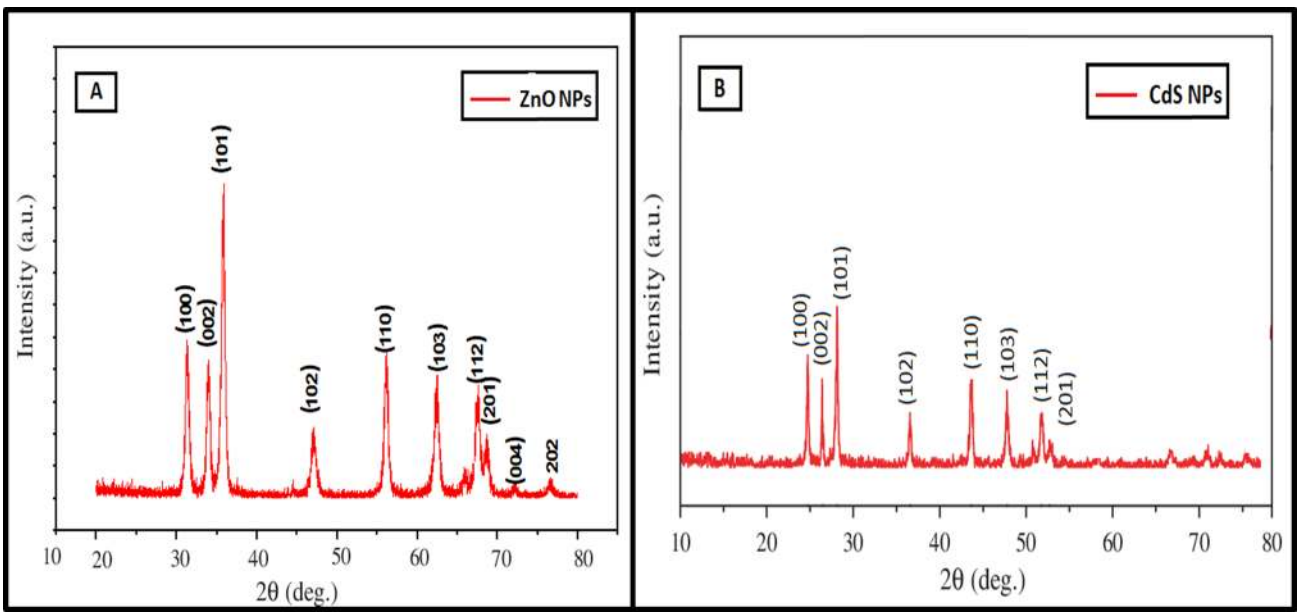


Fig. 6 XRD pattern of green synthesized **A** ZnO NPs and **B** CdS NPs

Table 1 Comparative summary of XRD, UV–Vis, and FTIR results for ZnO and CdS NPs

Technique	ZnO NPs	CdS NPs	Comparative interpretation
XRD phase	Hexagonal wurtzite ZnO	Hexagonal CdS	Both nanoparticle systems were successfully formed as crystalline hexagonal phases
Main XRD peaks	31.76°, 34.39°, 36.24°, 47.51°, 56.59°, 62.81°, 67.92°, 69.07°, 72.49°, 76.94°	24.8°, 26.5°, 28.1°, 36.6°, 43.6°, 47.8°, 51.8°	Peak positions confirm distinct ZnO and CdS crystal structures consistent with literature
Average crystallite size (XRD)	~31.2 nm	~41.28 nm	CdS showed a larger XRD-derived crystallite size than ZnO
UV–Vis absorption peak	~370 nm	~463 nm	ZnO absorbs mainly in the UV region, while CdS extends further into the visible region
Band-gap energy	3.29 eV	2.72 eV	CdS has a lower band gap, indicating higher visible-light response and potentially greater surface/electronic reactivity
FTIR broad O–H region	~3387.9 cm^{-1}	~3500 cm^{-1}	Both spectra indicate hydroxyl-containing surface species and/or adsorbed water
FTIR organic/surface functional groups	Peaks near 1436, 1004, 876 cm^{-1}	Peaks near 2358, 1452, 1389, 1100, 837 cm^{-1}	Both materials retain extract-related surface functionalities, suggesting plant-assisted surface stabilization
Fingerprint-region inorganic bands	Zn–O related bands near 471 and 400 cm^{-1}	Cd–S related bands near 601 and 570 cm^{-1}	These bands support successful formation of ZnO and CdS NPs
Overall interpretation	Crystalline UV-active oxide with smaller crystallite size	Crystalline visible-responsive sulfide with lower band gap	The two materials differ structurally and optically despite being produced by the same plant-assisted route

are depicted in Fig. 7 A. It can be observed that the majority of ZnO NPs fell within the nanometres scale, exhibiting spherical shapes with an average diameter ranging between 60–70 nm. Moreover, an agglomeration was observed among the ZnO NPs, a common feature in green-synthesized NPs owing to their higher surface area and the biomolecules as a capping agent which leads to aggregation of NPs [55]. This highlights the significant influence of ecological factors on NPs stability. The fabrication procedure of ZnO NPs depends on various growth parameters, including the concentration of plant extract, salt concentration, reaction duration, temperature, and solution pH. Consequently, careful calibration of these growth parameters is important to achieve the desired size and morphology of NPs, facilitating optimal manipulation.

The morphology of the CdS NPs was assessed through SEM analysis, as illustrated in Fig. 7 B. The resulting product consists of a large number of agglomerated NPs. SEM examination revealed a mean particle size for CdS ranging approximately between 30 and 50 nm. Conversely, the CdS NPs exhibit disparate shapes and sizes, suggesting a non-uniform nucleation process. According to particle size analysis, ZnO NPs have a narrower distribution with a mean diameter of 71.9 nm, Fig. 7 C. CdS NPs, on the other hand, show a change toward larger particle sizes with a greater mean size of 83.39 nm, Fig. 7D.

The purity of ZnO NPs was assessed through the use of energy dispersive X-ray analysis, as shown in Fig. 8A. The EDX spectrum shows the Zn and O peaks free of any impurities, confirming the presence of zinc and oxygen atoms in the sample. Additionally, the chemical components of Zn ONPs included a mass percentage of around 12.59% for O and 87.4% for Zinc. The atomic ratio percentage of Zn to O is almost 1.7. Additionally, the presence of Ag in the EDX spectrum is due to a thin silver coating on the ZnO NPs to enhance image quality. The elemental mapping of Zn ONPs, which shows the distribution of Zn and O with essentially no impurities, is shown in Fig. 8B.

Also, the EDX spectra of the CdS NP made with *Rhus coriorra* precursors are shown in Fig. 9A. The mass percentage of Cd and S in the synthesized NPs were 84.2% and 15.7%, respectively. The atomic ratio percentage of Cd to S is almost 1.5, as shown in Fig. 3. Furthermore, the elemental mapping distribution of CdS NPs, which shows the distribution of Cd and S with essentially no other elemental phases, as shown in Fig. 9 B. The EDX results confirmed that the synthesized CdS NPs are in a pure and stable state in nature [45].

The green synthesis mechanism of ZnO NPs was clarified through the demonstration using UV–vis and FT-IR techniques; these analyses collectively indicated the presence of reducing phytochemicals within the extract. The interaction of these phytochemicals with the precursor materials facilitated the green synthesis of ZnO NPs. The proposed mechanism is depicted in Fig. 10 A, it shows that in the ZnO system, the alkaline environment provided by NaOH is the most important factor. It speeds up the hydrolysis of Zn^{2+} ions and the formation of intermediates, including zinc hydroxide. These intermediates are converted to ZnO during drying and calcination. In these circumstances, the *R. coriaria* extract has capping/stabilizing effects. So, in the CdS system as illustrated in Fig. 10 (B), the reaction

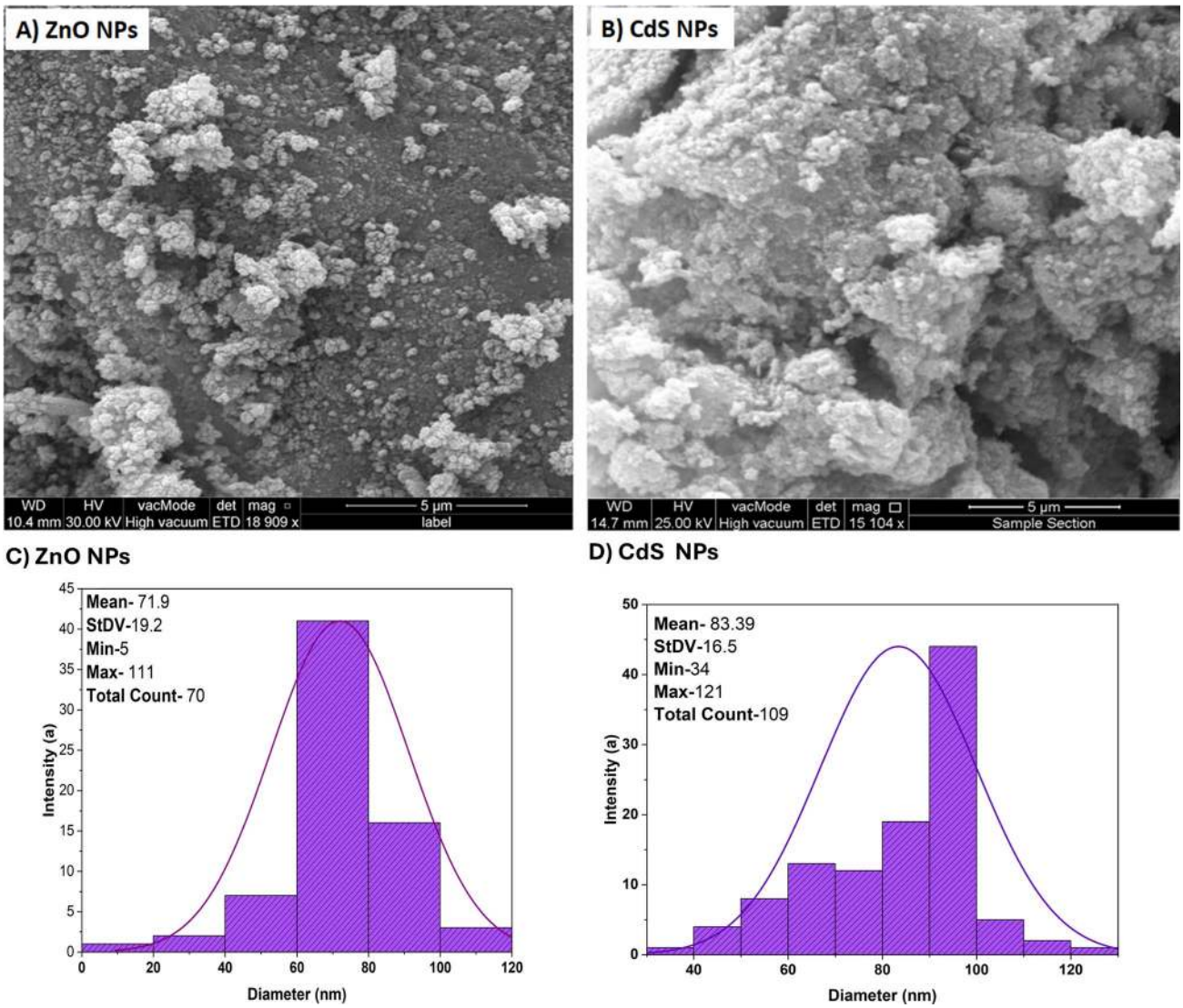


Fig. 7 The SEM images of green synthesized **A** ZnO NPs and **B** CdS NPs; the histogram of mean nanoparticles size distributions of **C** ZnO NPs and **D** CdS NPs

between Cd^{2+} ions and sulfide ions from Na_2S is what essentially causes NPs to form. This leads to the nucleation and development of CdS. Once again, it's more likely that the plant extract helps by controlling nucleation and stabilizing the NPs surface, rather than being the only way to make them. Consequently, pH, precursor chemistry, and sulfide availability are the primary determinants of NPs production, whereas the plant extract mostly serves as a biogenic coordinating and stabilizing medium.

The spherical shape and small particle size are promoted so that the materials will exhibit promising photocatalytic and antibacterial properties. Additionally, a review of the literature on plant extracts revealed that the *R. coriaria* extract included reducing and capping phytochemicals that, in accordance with the proposed mechanism, led to the production of CdS NPs, Fig. 10 B [46].

3.2 Antimicrobial Activities of Green Synthesized of CdS and ZnO NPs

3.2.1 Antibacterial Activity

The zone of inhibition was measured to examine the antibacterial activity of green synthesized CdS and ZnO NPs against antibiotic-resistant pathogens, including both Gram-positive bacteria (*S. aureus*) and Gram-negative bacteria (*K. pneumoniae* and *P. aeruginosa*) (Table 1). The results showed that the CdS and ZnO NPs have strong antibacterial activity. The increasing diameter of the inhibition zone demonstrated that higher NPs concentrations enhanced antibacterial activity Fig. 11. The positive controls showed that Amoxicillin exhibited no antibacterial activity, while Chloramphenicol produced strong inhibition against *K.*

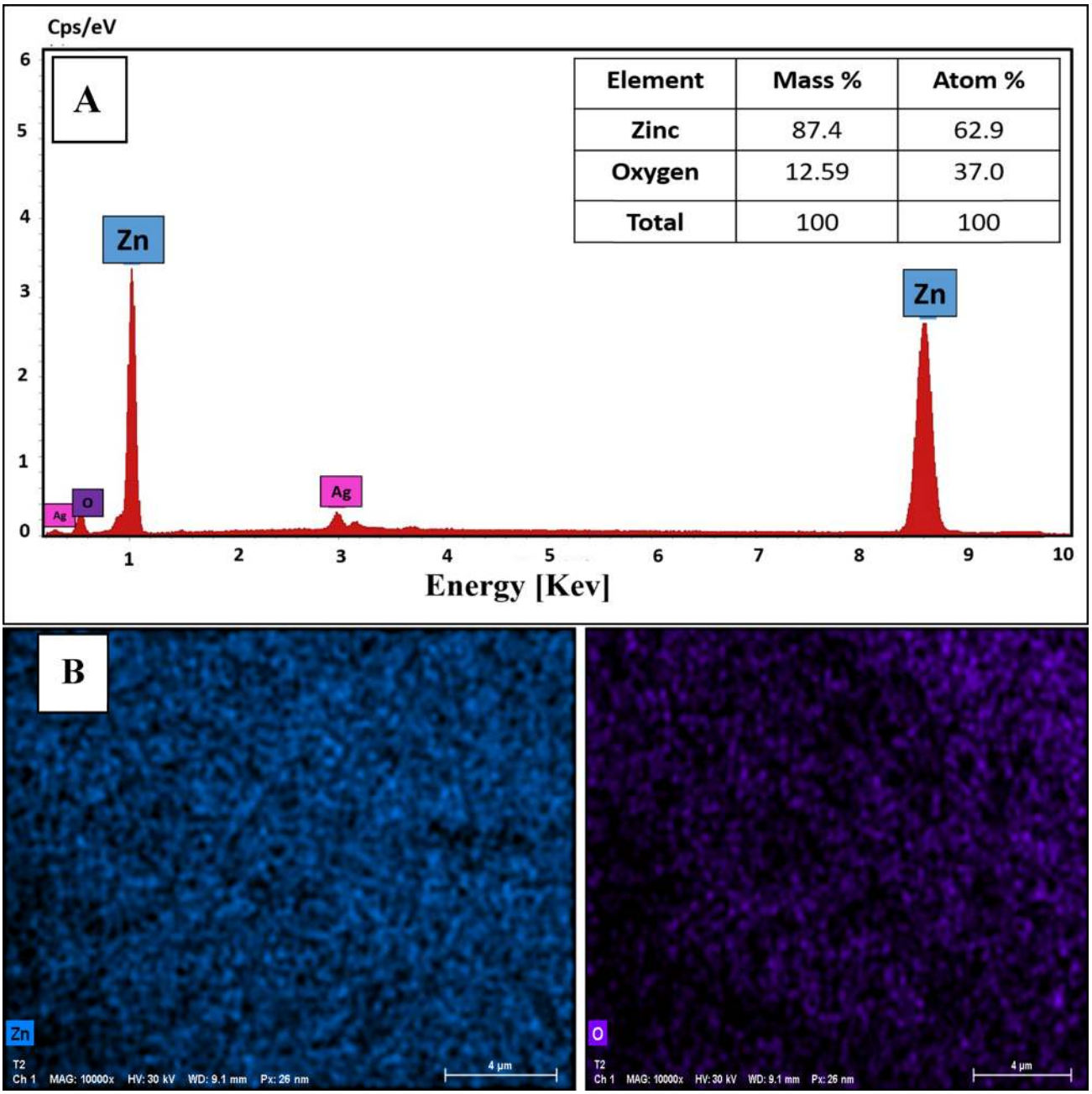
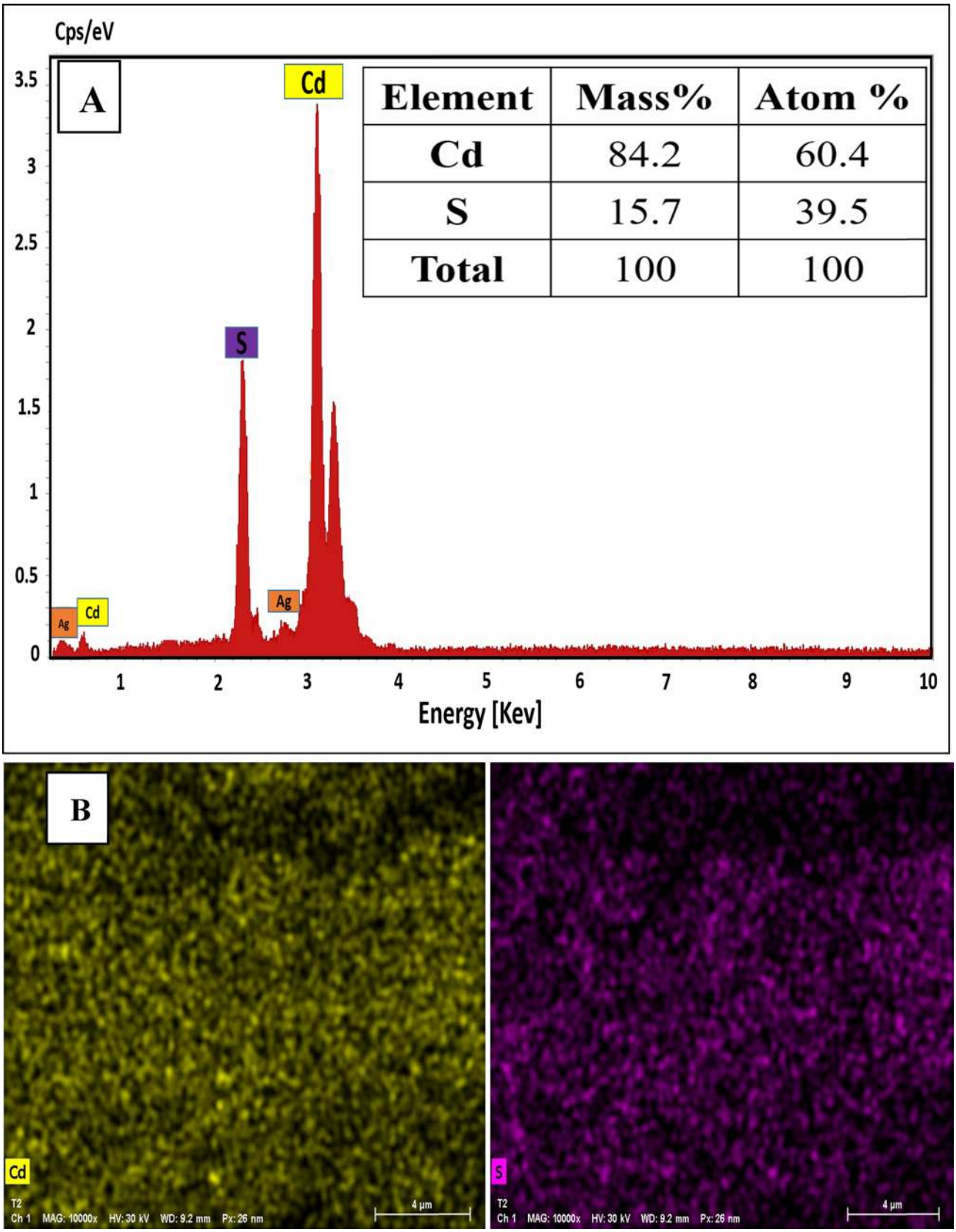


Fig. 8 EDX analysis of **A** ZnO NPs and **B** elemental mapping distribution of ZnO NPs

pneumoniae and *S. aureus*, but not *P. aeruginosa*.as shown in Table 2 and Fig. 13. The comparison shows that the antimicrobial activity of NPs in our study is generally higher than or comparable to previous reports. ZnO NPs exhibited similar or slightly lower activity, with some resistance observed, whereas CdS NPs in our study demonstrated significantly larger inhibition zones and broader-spectrum effects, particularly against *K. pneumoniae*, and *S. aureus*, indicating improved efficacy relative to earlier studies, as shown in Table 3.

The rise in antibiotic-resistant bacteria in recent years has been attributed to the misuse and overuse of broad-spectrum antibiotics, such as Methicillin-resistant *S. aureus* [47].

Generally, the way that the NPs impact bacteria is by a reaction between the positive ions from the metals in the particles and the negative ions present in the bacterial structure [48]. Because this interaction affects the thiol proteins in bacterial cell membranes, it causes oxidative stress events and bacterial membrane oxidation [49]. For instance, a variety of approaches have been developed to assess how ZnO NPs work against bacteria. Among these interactions are



Element	Mass%	Atom %
Cd	84.2	60.4
S	15.7	39.5
Total	100	100

Fig. 9 EDX analysis of **A** CdS NPs and **B** elemental mapping distribution of CdS NPs

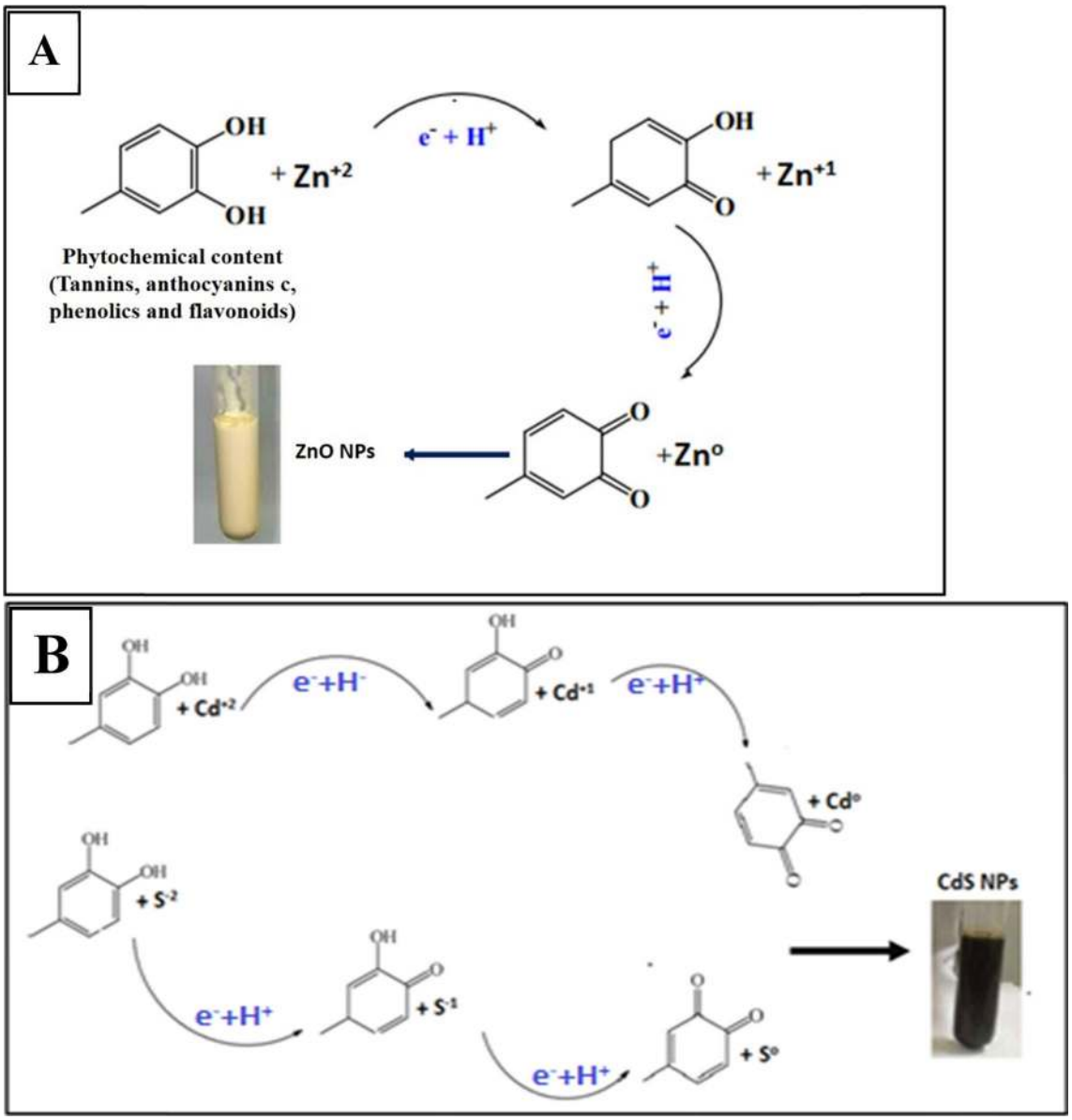


Fig. 10 Proposed mechanism for green synthesis **A** ZnO and **B** CdS NPs

chemical reactions between cell membrane molecules and Zn^{+2} ions [50–52]. After passing through the membrane and entering the cell, ions have the ability to chemically react with intracellular materials, destroying intracellular components, Fig. 14. ZnO NPs can generate H_2O_2 in the environment, once formed, it can interact with the chemical components of cell membranes. ZnO NPs also damage cells by obstructing electron transfer, decreasing the coating and membrane physically through abrasion and corrosion, and obstructing cell membrane transmission channels [52, 53].

3.2.2 Antifungal Activity

The findings show that all tested concentrations of the CdS NPs have strong antifungal activity against *C. albicans* while the fungi have resistance to the ZnO NPs. Interestingly, the inhibition zone increased in a dose-dependent manner with CdS NPs, with statistically significant differences compared to the ZnO NPs as the highest concentration (100 mg/mL) produced a zone of inhibition of 29 ± 1.2 mm. On the other hand, the anti-candidal activity of ZnO NPs at all studied concentrations does not exhibit any inhibitory zone, (Fig. 12 and Table 3), suggesting that *C. albicans* has a defense mechanism against ZnO NPs. This resistance could be due to the structural properties of *C. albicans*, which may

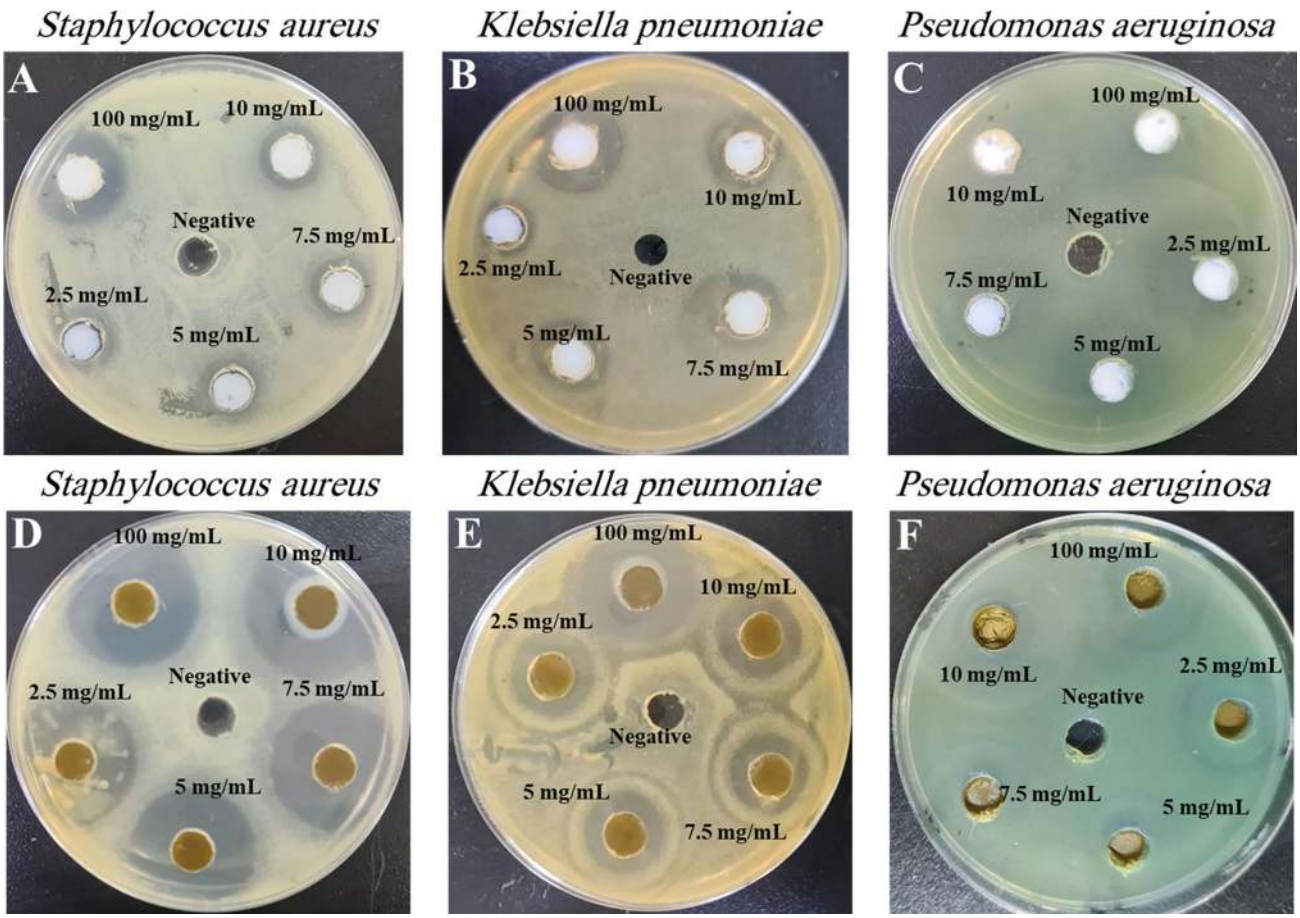


Fig. 11 Qualitative antibacterial activity of ZnO NPs **A, B & C** and CdS NPs **D, E & F** with S.aureus, K.pneumoniae, and P.aeruginosa

Table 2 Quantitative antibacterial activity of ZnO and CdS NPs

NPs Concentrations (mg/mL)	Inhibition zone (mm)		
	K. pneumoniae	*S. aureus*	*P. aeruginosa*
Negative (C)	R	R	R
ZnO NPs			
2.5	12.6 ± 0.8	11.7 ± 0.85	R
5	13.7 ± 1.35	12.9 ± 0.95	R
7.5	15.7 ± 0.85	14.3 ± 1.15	R
10	17 ± 0.5	15.7 ± 0.85	R
100	22.2 ± 0.6	23.4 ± 0.3	R
CdS NPs			
2.5	21.0 ± 0.5*	29.1 ± 0.45 *	R
5	22 ± 1.0 *	27.2 ± 0.4 *	R
7.5	23 ± 0.5 *	28.3 ± 0.35 *	R
10	26 ± 0.5*	30.7 ± 0.35 *	R
100	32.1 ± 1.05*	33.2 ± 0.6 *	15.5 ± 0.3 *
Positive control (Amoxicillin)	R	R	R
Positive control (Chloramphenicol)	26 ± 0.4 *	36 ± 0.65 *	R

The data were represented as (mean ± SE), One–Way ANOVA were used to compare the means between each bacterial species treated with CdS NPs and ZnO NPs, * (p value < 0.05)

Table 3 Quantitative antifungal activity in (means ± SE) of CdS and ZnO NPs against C. albicans

Concentrations of NPs (mg/mL)	Zone inhibition (mm)	
	CdS NPs	ZnO NPs
Negative (C)	R	R
2.5	18.0 ± 2.0	R
5	18.0 ± 0.5	R
7.5	20.0 ± 0.25	R
10	23.0 ± 0.5	R
100	29.0 ± 1.2	R
Positive control (Fluconazole)	21.0 ± 0.5	21.0 ± 0.5
Positive control (miconazole)	45.0 ± 0.5	45.0 ± 0.5

prevent ZnO NPs from effectively interacting with and disrupting the fungal cell membrane [54].

The positive controls, Fluconazole and Miconazole, showed moderate and strong inhibition, respectively. Compared to ZnO NPs, in Fig. 11 the CdS NPs exhibited comparable or higher activity at high concentrations (Table 2 and Fig. 13). Compared to other studies, CdS NPs in our study showed higher antifungal activity against *C. albicans* (23 mm) than previously reported values (14–22.5 mm), while ZnO NPs demonstrated weaker or no activity as shown in Table 4.

CdO NPs are essential in biomedical applications because of their antimicrobial qualities. These microstructures have demonstrated their strong antibacterial and antifungal resistance to bacterial and fungal illnesses because of the presence of ROS, the release of cadmium Cd^{2+} ions, and the size and shape of the material NPs, Fig. 14 [55]. The antifungal activity of CdS NPs indicates that they can interact with and damage the cell membrane of *C. albicans* cells [56]. On the fungal cells' surface, pits and pores have formed, suggesting that the CdS NPs may damage the membrane and trigger cell death. This process is consistent with earlier research showing that the main mechanism of antifungal action is cell membrane disruption caused by NPs [57, 58].

Cadmium possesses unique physicochemical properties, including high electrical conductivity, corrosion resistance, flexibility, and malleability [59]. However, it has no known biological function and is well recognized for its toxicity to humans. Cd accumulation in tissues can induce oxidative stress by generating reactive oxygen species (ROS), disrupt antioxidant defense systems, and lead to adverse health effects. Although cadmium sulfide (CdS) exhibits advantageous optical, electrical, and photocatalytic properties and is reported to have relatively lower toxicity compared to elemental cadmium, potential toxic effects cannot be ignored [60]. Therefore, its application, particularly in biomedical fields, should be approached with caution and supported by comprehensive toxicity assessments [24].

The antibacterial properties exhibited in this work can be analyzed in terms of the physicochemical attributes of the produced NPs. XRD results showed that both ZnO and CdS NPs were crystalline hexagonal phases, although their optical and morphological features were different. CdS had a smaller band-gap energy (2.72 eV) than ZnO (3.29 eV), which could make it more reactive on the surface and lead to stronger antibacterial effects through oxidation or ion transfer. Also, SEM analysis showed that ZnO particles were more highly agglomerated and had a greater apparent size range (approximately 31.2 nm), whereas CdS particles were smaller (about –41.28 nm). This could make the surface area accessible for contact with microbial cell envelopes more effective. FTIR spectra for both materials also showed the presence of hydroxyl and organic functional groups on the surface, originating from the extract. These groups could affect how NPs stay stable, spread out, and come into touch with bacterial or fungal cells. These combined physicochemical differences explain why CdS had stronger antibacterial activity and a distinct antifungal effect against Candida albicans. On the other hand, the more agglomerated ZnO NPs had lesser activity and no apparent antifungal effect under the investigated conditions.

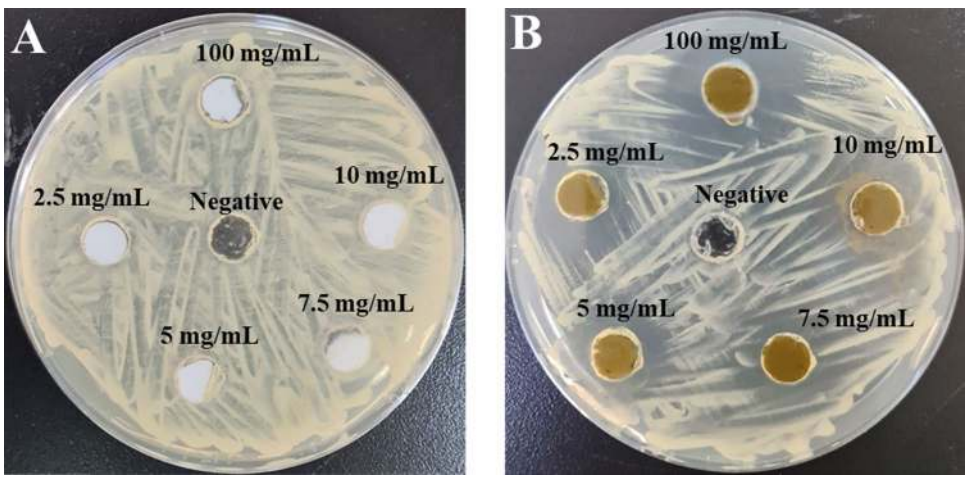


Fig. 12 Qualitative antifungal activity against *C. albicans*, **A** ZnO NPs, **B** CdS NPs

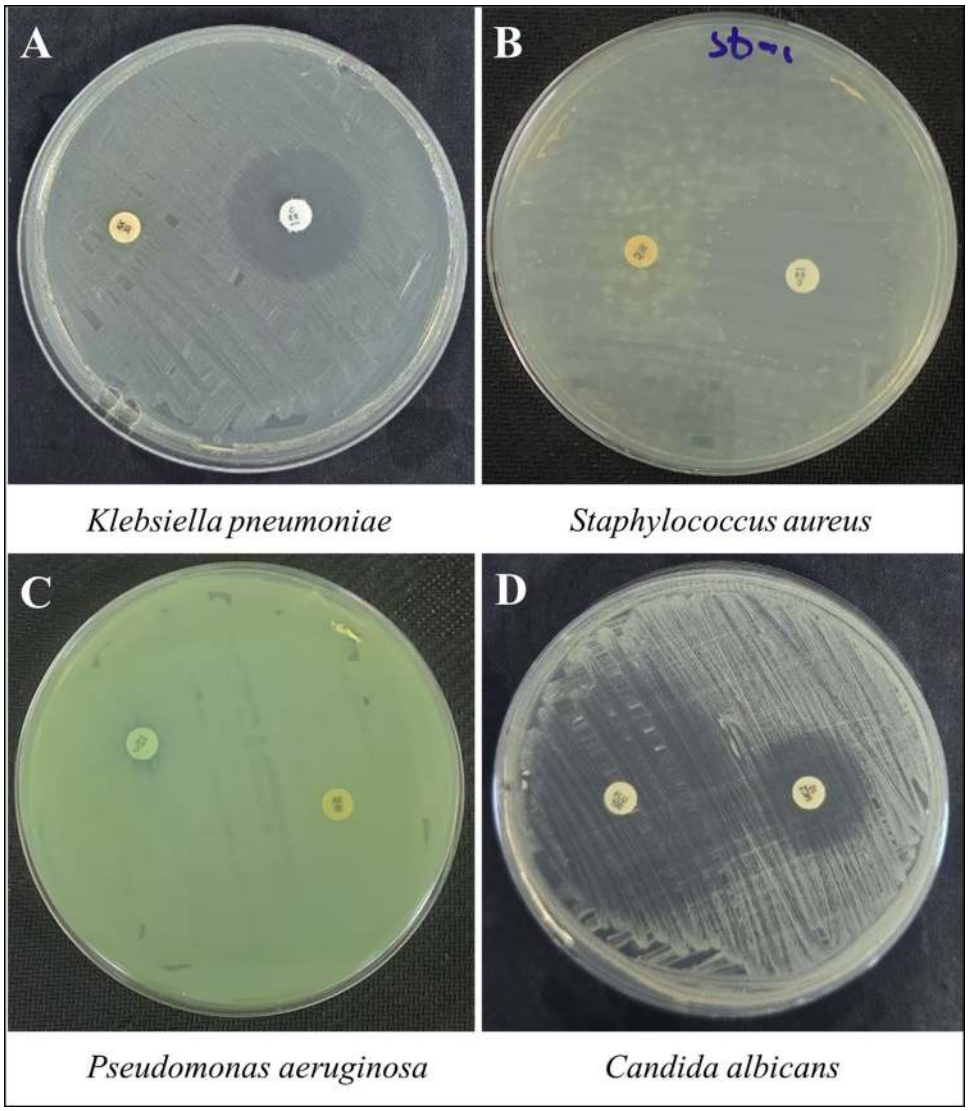


Fig. 13 Qualitative antifungal activity of the antimicrobials as positive controls against the bacteria and fungus. **A***K. pneumoniae*, **B***S.aureus*, **C***P. aeruginosa*, **D***C. albicans*

4 Conclusions

The study successfully utilized *R. coriaria* extract as a green biosynthetic medium for the synthesis of ZnO and CdS NPs. Structural and optical characterization by XRD, UV–Vis, FTIR, SEM, and EDX confirmed the successful formation of both nanomaterials with hexagonal crystalline structures. It was found that the optical band-gap values were 3.29 eV for ZnO and 2.72 eV for CdS. XRD analysis showed that the average crystal sizes were 31.2 nm for ZnO and 41.28 nm for CdS. SEM showed that the particles were agglomerated. Biological assessment revealed that both NPs displayed concentration-dependent antibacterial activity, whereas CdS NPs exhibited distinct antifungal activity against *C. albicans*, unlike ZnO under the same conditions. In general, the results show that producing NPs from *R. coriaria* is an environmentally benign approach with significant antimicrobial potential. However, the current study is preliminary, and future studies should focus on optimizing synthesis conditions, yield, and batch reproducibility; BET surface area analysis; detailed antimicrobial determination; and thorough toxicity evaluation.

Table 4 Comparison of antimicrobial activity of ZnO and CdS NPs against selected microorganisms in this study and previous reports

Types of the NPs	Zone of the inhibition (mm)				References
	K. pneumoniae	*S. aureus*	*P. aeruginosa*	*C. albicans*	
ZnO	–	21	21	–	[61]
ZnO	–	31	17	–	[62]
ZnO	17	–	–	–	[63]
ZnO	23	–	–	–	[64]
ZnO	–	R	–	–	[65]
ZnO	–	–	–	14	[66]
ZnO	–	–	–	22.5	[67]
ZnO	17	16	R	R	Our study
CdS NPs		25	–	R	[68]
CdS/Fe3O4 NCs	26	–	22	–	[69]
CdS NPs	–	10	–	–	[70]
CdSNPs	21	24	21	–	[71]
CdSNPs	–	–	13.6	–	[72]
CdSNPs	–	17	–	–	[73]
CdSNPs	26	30	R	23	Our study
Ag/CuO NCs	–	36.1	–	–	[74]
CuO NPs	–	27	–	–	[75]

(–) means not available in the study

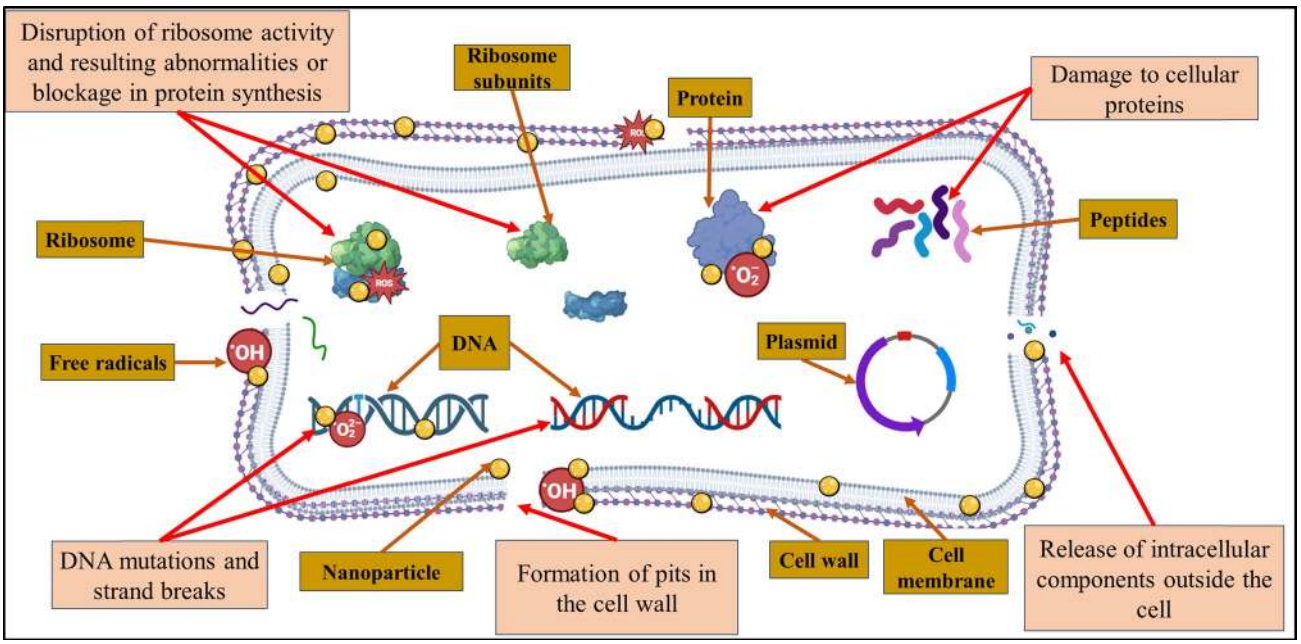


Fig. 14 Schematic illustration for antimicrobial properties of the green synthesized NPs

Supplementary Information The online version contains supplementary material available at https://doi.org/10.1007/s10904-026-04318-5.

Author Contribution S.H.; Conceptualization, Supervision, Writing – original draft. D.H.M; Synthesis, Characterisation, Formal analysis, Methodology, Writing – original draft. R.M.M.; Anti-Microbial Measurements, Formal analysis, Writing – review & editing. P.J.J.; Anti-Becterial and Anti-Fungal Investigation, Validation, P.A.; Characterisation, Project administration, Writing – review & editing. D.S.; Conceptualisation, Resources, Supervision, Writing – review & editing.

Funding This study conducted without receiving any funds.

Data Availability No datasets were generated or analysed during the current study.

Declarations

Competing Interests The authors declare no competing interests.

Ethical Approval Not applicable.

Open Access This article is licensed under a Creative Commons Attribution 4.0 International License, which permits use, sharing, adaptation, distribution and reproduction in any medium or format, as long as you give appropriate credit to the original author(s) and the source, provide a link to the Creative Commons licence, and indicate if changes were made. The images or other third party material in this article are included in the article's Creative Commons licence, unless indicated otherwise in a credit line to the material. If material is not included in the article's Creative Commons licence and your intended use is not permitted by statutory regulation or exceeds the permitted use, you will need to obtain permission directly from the copyright holder. To view a copy of this licence, visit http://creativecommons.org/licenses/by/4.0/.

References

1. K. Selvam, A. Ragu Prasath, A.K. Alanazi, A review of recent developments in green synthesis of silver nanoparticles: antioxidant and antibacterial applications. Microsc. Res. Tech. **89**(1), 134–147 (2026)
2. A. Saravanan, P.S. Kumar, S. Karishma, D.-V.N. Vo, S. Jeevanantham, P. Yaashikaa et al., A review on biosynthesis of metal nanoparticles and its environmental applications. Chemosphere. **264**, 128580 (2021)
3. N. Baig, I. Kammakakam, W. Falath, Nanomaterials: a review of synthesis methods, properties, recent progress, and challenges. Mater. Adv. **2**(6), 1821–1871 (2021)
4. N. Rodríguez-Barajas, M.D. Ponce-Regalado, M.S. Segura-Almendárez, C.M. Rodríguez-Razon, S. Ghotekar, M. Fellah et al., Plant-mediated synthesis and interaction of ZnO against breast and prostate cancer: review. Results Chem. **9**, 101654 (2024)
5. S.M.S. Abo El-Souad, M.A. Ramadan, D. Zahran, Synthesis and application of Cobalt-Silver nanohybrid for antimicrobial wastewater treatment and agricultural productivity enhancement. Sci. Rep. **15**(1), 16321 (2025)
6. D. Chen, X. Liu, X. Lu, J. Tian, Nanoparticle drug delivery systems for synergistic delivery of tumor therapy. Front. Pharmacol. (2023). https://doi.org/10.3389/fphar.2023.1111991
7. J. Trzcińska-Wencel, N. Mucha, M. Rai, J. Tyburski, P. Golińska, Pre-sowing grain treatment with bio-AgNPs stimulates plant growth and affects redox homeostasis in maize. Front. Plant Sci. **16**, 1494741 (2025)
8. H. Kumar, K. Kuča, S.K. Bhatia, K. Saini, A. Kaushal, R. Verma et al., Applications of Nanotechnology in Sensor-Based Detection of Foodborne Pathogens. Sensors. **20**(7), 1966 (2020)
9. K.A. Altammar, A review on nanoparticles: characteristics, synthesis, applications, and challenges. Front. Microbiol. **14**, 1155622 (2023)
10. A.M. El-Khawaga, A. Zidan, A.I.A.A. El-Mageed, Preparation methods of different nanomaterials for various potential applications: a review. J. Mol. Struct. **1281**, 135148 (2023)
11. A. Dhaka, S. Chand Mali, S. Sharma, R. Trivedi, A review on biological synthesis of silver nanoparticles and their potential applications. Results Chem. **6**, 101108 (2023)
12. P.B. Chouke, T. Shrirame, A.K. Potbhare, A. Mondal, A.R. Chaudhary, S. Mondal et al., Bioinspired metal/metal oxide nanoparticles: A road map to potential applications. Mater. Today Adv. **16**, 100314 (2022)
13. S. kazemi, A. Hosseingholian, S.D. Gohari, F. Feirahi, F. Moammeri, G. Mesbahian et al., Recent advances in green synthesized nanoparticles: from production to application. Mater. Today Sustain. **24**, 100500 (2023)
14. A.S. Kadhim, Z.S.A. Al-Ali, Green synthesis of reduced Graphene Oxide nanosheets using Iraqi *Rhus coriaria* (L.) fruits extract and a study of its anticancer activity. Iraqi J. Sci. **65**(11), 6253–6266 (2024)
15. P.S. Bapte, S. Pansambal, P.P. Bardapurkar, S. Ghotekar, S.S. Borgave, Eco-friendly synthesis of ZnO nanoparticles using pomegranate leaves and its antimicrobial, antioxidant, anticancer, angiogenic activity, and toxicity assessment. Results Chem. **16**, 102460 (2025)
16. R. Abali, I. Temel Yuksel, M.A. Yuksel, B. Bulut, M. Imamoglu, V. Emirdar et al., Implications of circulating irisin and Fabp4 levels in patients with polycystic ovary syndrome. J. Obstet. Gynaecol. **36**(7), 897–901 (2016)
17. Z.A. Elagbar, A.K. Shakya, L.M. Barhoumi, H.I. Al-Jaber, Phytochemical diversity and pharmacological properties of *Rhus coriaria*. Chem. Biodivers. **17**(4), e1900561 (2020)
18. H. Alsamri, K. Athamneh, G. Pintus, A.H. Eid, R. Iratni, Pharmacological and antioxidant activities of *Rhus coriaria* L. (sumac). Antioxidants **10**(1), 73 (2021)
19. S. Medici, M. Peana, A. Pelucelli, M.A. Zoroddu (eds.). *An updated overview on metal nanoparticles toxicity*. Seminars in cancer biology (Elsevier, 2021)
20. S. Antunes Filho, M.S. dos Santos, O.A.L. dos Santos, B.P. Backx, M.-L. Soran, O. Opriş et al., Biosynthesis of nanoparticles using plant extracts and essential oils. Molecules **28**(7), 3060 (2023)
21. R.A. Al-Refaia, Z.S. Al-Ali, E. Alrikabi, F.M. Alkhatib, Biogenic synthesis of multifunctional Zinc Oxide nanoparticles using *Rosmarinus officinalis* L. extract: comprehensive evaluation of antibacterial, antioxidant, and antimalarial potential. Rev. Colomb. Quím. **54**(2), 3 (2025)
22. A.A. Yaqoob, H. Ahmad, T. Parveen, A. Ahmad, M. Oves, I.M.I. Ismail et al., Recent advances in metal decorated nanomaterials and their various biological applications: a review. Front. Chem. (2020). https://doi.org/10.3389/fchem.2020.00341
23. E. Vidhya, S. Vijayakumar, S. Prathipkumar, P.K. Praseetha, Green way biosynthesis: characterization, antimicrobial and anticancer activity of ZnO nanoparticles. Gene Rep. **20**, 100688 (2020)
24. A. Ghasempour, H. Dehghan, M. Ataee, B. Chen, Z. Zhao, M. Sedighi et al., Cadmium sulfide nanoparticles: preparation, characterization, and biomedical applications. Molecules **28**(9), 3857 (2023)
25. B.H. Shnawa, P.J. Jalil, S.M. Hamad, M.H. Ahmed, Antioxidant, protoscolicidal, hemocompatibility, and antibacterial activity of nickel oxide nanoparticles synthesized by *Ziziphus spina-christi*. BioNanoScience **12**(4), 1264–1278 (2022)
26. M.I. Rahmah, H.B. Qasim, A novel method to prepare antibacterial ZnO nanoflowers. Appl. Phys. A **128**(11), 998 (2022)
27. P.J. Jalil, R.M. Mhamedsharif, B.H. Shnawa, S.M. Hamad, P. Aspoukeh, K.W. Wsu et al., Biosynthesis of ZnO nanoparticles using washingtonia filifera seed extract and assessment of their anti-inflammatory and antimicrobial efficacy. J. Cluster Sci. **36**(1), 31 (2024)
28. L. Motelica, B.-S. Vasile, A. Ficai, A.-V. Surdu, D. Ficai, O.-C. Oprea et al., Antibacterial activity of zinc oxide nanoparticles loaded with essential oils. Pharmaceutics. **15**(10), 2470 (2023)
29. I. Khan, K. Saeed, I. Khan, Nanoparticles: properties, applications and toxicities. Arab. J. Chem. **12**(7), 908–931 (2019)
30. H. Dabhane, S. Ghotekar, P. Tambade, S. Pansambal, H.C.A. Murthy, R. Oza et al., A review on environmentally benevolent synthesis of CdS nanoparticle and their applications. Environ. Chem. Ecotoxicol. **3**, 209–219 (2021)
31. M.J. Bhat, M. Al-Qahtani, A.S. Badawi, G.B. Asiri, A.M. Alhmare, A. Rashid et al., Awareness and knowledge of antibiotic resistance and risks of self-medication with antibiotics among

the Aseer Region Population, Saudi Arabia, 2023. Cureus. **15**(6), e40762 (2023)
32. H. Lv, M. Yang, Y. Yang, Z. Tang, Y. Guo, J. Zhou et al., Metal ion and antibiotic co-loaded nanoparticles for combating methicillin-resistant *Staphylococcus aureus*-induced osteomyelitis. ACS Nano **19**(5), 5253–5268 (2025)
33. R.M. Mhammedsharif, P.J. Jalil, K.W. Wsu, S.M.M. Sharif, M.H. Ahmed, Eco-friendly fabrication of Ag-ZnO nanocomposites from *Adiantum capillus-veneris*: targeting biofilms and resistant microbes. Total Environ. Eng. **5**, 100053 (2025)
34. A. Kakanejadifard, V. Khojasteh, A. Zabardasti, F. Azarbani, New Azo-Schiff base ligand capped silver and cadmium sulfide nanoparticles preparation, characterization, antibacterial and antifungal activities. Org. Chem. Res. **4**(2), 210–226 (2018)
35. L. Nobs, F. Buchegger, R. Gurny, E. Allémann, Surface modification of poly(lactic acid) nanoparticles by covalent attachment of thiol groups by means of three methods. Int. J. Pharm. **250**(2), 327–337 (2003)
36. S.M. Mustafa, A.A. Barzinjy, A.H. Hamad, S.M. Hamad, Betaine-based deep eutectic solvents mediated synthesis of zinc oxide nanoparticles at low temperature. JCI **48**(19), 28951–28960 (2022)
37. H. Richter, Z. Wang, L.J. Ley, The one phonon Raman spectrum in microcrystalline silicon. Sms **180**, 257–261 (2005)
38. T. Cun, C. Dong, Q. Huang, Ionothermal precipitation of highly dispersive ZnO nanoparticles with improved photocatalytic performance. Appl. Surf. Sci. **384**, 73–82 (2016)
39. H.S. Mahdi, A. Parveen, S. Agrawal, A. Azam (eds), *Microstructural and optical properties of sol gel synthesized CdS nano particles using CTAB as a surfactant*. AIP conference proceedings (AIP Publishing, 2017)
40. M.R. Hosseini, M.N. Sarvi, Recent achievements in the microbial synthesis of semiconductor metal sulfide nanoparticles. JMSiSP **40**, 293–301 (2015)
41. N. Susha, K. Nandakumar, S.S. Nair, Enhanced photoconductivity in CdS/betanin composite nanostructures. RSC Adv. **8**(21), 11330–11337 (2018)
42. A.A. Barzinjy, S.M. Hamad, A.F. Abdulrahman, S.J. Biro, A.A. Ghafor, Biosynthesis, characterization and mechanism of formation of ZnO nanoparticles using *Petroselinum crispum* leaf extract. JCOS **17**(7), 558–566 (2020)
43. S. Pandya, K. Raval, Investigation of structural, morphological and optical properties of cadmium sulphide (CdS) thin films at different Cd/S concentration deposited by chemical technique. JJoMSMiE **28**(23), 18031–18039 (2017)
44. S.A. Speakman, Estimating crystallite size using XRD. MIT Center Mater. Sci. Eng. **2**(14), 03–08 (2014)
45. A. Regmi, Y. Basnet, S. Bhattarai, S.K. Gautam, Cadmium sulfide nanoparticles: synthesis, characterization, and antimicrobial study. J. Nanomater. (2023). https://doi.org/10.1155/2023/8187000
46. B.S. Goud, Y. Suresh, S. Annapurna, A. Singh, G. Bhikshamaiah, Green synthesis and characterization of cadmium sulphide nanoparticles. JMTP **3**(10), 4003–4008 (2016)
47. D.I. Andersson, D. Hughes, Microbiological effects of sublethal levels of antibiotics. Nat. Rev. Microbiol. **12**(7), 465–478 (2014)
48. R. Muksy, K. Kolo, S.M. Gorony, Bacterial and fungal-mineral interactions and their application in bioremediation – a review. J. Ecol. Eng. **24**(5), 1–13 (2023)
49. V. Pareek, S. Devineau, S.K. Sivasankaran, A. Bhargava, J. Panwar, S. Srikumar et al., Silver nanoparticles induce a triclosan-like antibacterial action mechanism in multi-drug resistant *Klebsiella pneumoniae*. Front. Microbiol. **12**, 638640 (2021)
50. M. Roberson, V. Rangari, S. Jeelani, T. Samuel, C. Yates, Synthesis and characterization silver, zinc oxide and hybrid silver/zinc oxide nanoparticles for antimicrobial applications. Nano Life **4**(01), 1440003 (2014)
51. K. Elumalai, S. Velmurugan, Green synthesis, characterization and antimicrobial activities of zinc oxide nanoparticles from the leaf extract of *Azadirachta indica* (L.). Appl. Surf. Sci. **345**, 329–336 (2015)
52. A. Sirelkhatim, S. Mahmud, A. Seeni, N.H.M. Kaus, L.C. Ann, S.K.M. Bakhori et al., Review on zinc oxide nanoparticles: antibacterial activity and toxicity mechanism. Nano-micro letters. **7**, 219–242 (2015)
53. C. Guo, J. Xue, Y. Dong, Fabrication and characterization of hydroxyapatite nanomaterial dual deposited with nano silver and zinc oxide. Mater. Lett. **219**, 182–185 (2018)
54. S. Bhattacharya, S. Sae-Tia, B.C. Fries, Candidiasis and mechanisms of antifungal resistance. Antibiotics (Basel, Switzerland). **9**(6), 312 (2020)
55. A.Z. Skheel, M.H. Jaduaa, A.N. Abd, Green synthesis of cadmium oxide nanoparticles for biomedical applications (antibacterial, and anticancer activities). Mater. Today Proc. **45**, 5793–5799 (2021)
56. S. Adhikari, K. Parajuli, G.B. Karki, S.P. Khatiwada, R. Adhikari, Structural, optical and antimicrobial properties of carbohydrate-capped cadmium sulfide nanoparticles. J. Nepal Chem. Soc. **43**(2), 1–10 (2023)
57. C. Malarkodi, S. Rajeshkumar, K. Paulkumar, M. Vanaja, G. Gnanajobitha, G. Annadurai, Biosynthesis and antimicrobial activity of semiconductor nanoparticles against oral pathogens. Bioinorg. Chem. Appl. **2014**, 347167 (2014)
58. R. Muksy, K. Kolo, Experimental observations and assessment of landfill leachate bioremediation by autochthonous fungi species and their effective geoactivities. J. Ecol. Eng. **24**(1), 312–327 (2023)
59. X. Zheng, Y. Liu, Y. Yang, Y. Song, P. Deng, J. Li et al., Recent advances in cadmium sulfide-based photocatalysts for photocatalytic hydrogen evolution. Renewables. **1**(1), 39–56 (2023)
60. M. Huang, C. Liu, P. Cui, T. Wu, X. Feng, H. Huang et al., Facet-dependent photoinduced transformation of cadmium sulfide (CdS) nanoparticles. Environ. Sci. Technol. **55**(19), 13132–13141 (2021)
61. E. Hoseinzadeh, M.-Y. Alikhani, M.-R. Samarghandi, M. Shirzad-Siboni, Antimicrobial potential of synthesized zinc oxide nanoparticles against gram positive and gram negative bacteria. Desalin. Water Treat. **52**(25), 4969–4976 (2014)
62. A.A. Tayel, W.F. El-Tras, S. Moussa, A.F. El-Baz, H. Mahrous, M.F. Salem et al., Antibacterial action of zinc oxide nanoparticles against foodborne pathogens. J. Food Saf. **31**(2), 211–218 (2011)
63. S. Asokan, T. Jacob, T. Cherian, A.A. AlSosowaa, F.Q. Al-Mojahid, S. Vijayan, Biogenic ZnO nanoparticles from *Bacillus amyloliquefaciens* NWR-14 for combating ESBL-producing *Klebsiella pneumoniae*. Biomed. Mater. Devices. (2026). https://doi.org/10.1007/s44174-026-00635-y
64. E. Rasha, A. Monerah, A. Manal, A. Rehab, D. Mohammed, E. Doaa, Biosynthesis of zinc oxide nanoparticles from *Acacia nilotica* (L.) extract to overcome carbapenem-resistant *Klebsiella pneumoniae*. Molecules **26**(7), 1919 (2021)
65. M. Banoee, S. Seif, Z.E. Nazari, P. Jafari-Fesharaki, H.R. Shahverdi, A. Moballegh et al., ZnO nanoparticles enhanced antibacterial activity of ciprofloxacin against Staphylococcus aureus and *Escherichia coli*. J. Biomed. Mater. Res. B Appl. Biomater. **93B**(2), 557–561 (2010)
66. M.A. Abomuti, E.Y. Danish, A. Firoz, N. Hasan, M.A. Malik, Green synthesis of zinc oxide nanoparticles using salvia officinalis leaf extract and their photocatalytic and antifungal activities. Biology. **10**(11), 1075 (2021)
67. M.T. Yassin, F.O. Al-Otibi, A.A. Al-Askar, M.M. Elmaghrabi, Synergistic anticandidal effectiveness of greenly synthesized zinc

oxide nanoparticles with antifungal agents against nosocomial candidal pathogens. Microorganisms. **11**(8), 1957 (2023)
68. M.S. Alsaggaf, A.F. Elbaz, S. El Badawy, S.H. Moussa, Anticancer and antibacterial activity of cadmium sulfide nanoparticles by *Aspergillus niger*. Adv. Polym. Technol. **2020**(1), 4909054 (2020)
69. R. Golabiazar, G.S. Qadir, Z.A. Faqe, K.M. Khalid, K.I. Othman, N.F. Rasool et al., Green biosynthesis of CdS NPs and CdS/Fe3O4 NCs by Hawthorn plant extract for photodegradation of methyl orange dye and antibacterial applications. J. Cluster Sci. **33**(3), 1223–1238 (2022)
70. A. Regmi, Y. Basnet, S. Bhattarai, S.K. Gautam, Cadmium sulfide nanoparticles: synthesis, characterization, and antimicrobial study. J. Nanomater. **2023**(1), 8187000 (2023)
71. N.J. Mohammed, G.J. Zylstra, T.Y. Mutter, Green synthesis of hyaluronic acid coated cadmium sulfide nanoparticles with enhanced antibacterial activity. Discov. Mater. **5**(1), 225 (2025)
72. A. Shivashankarappa, K.R. Sanjay, *Escherichia coli*-based synthesis of cadmium sulfide nanoparticles, characterization, antimicrobial and cytotoxicity studies. Braz. J. Microbiol. **51**(3), 939–948 (2020)
73. E.U. Ekwujuru, M.G. Peleyeju, C. Ssemakalu, M. Monapathi, M. Klink, Characterization and antimicrobial assessment of cadmium sulfide nanoparticles. Int. J. Mol. Sci. **27**(1), 432 (2026)
74. A.J. Mustafa, P.J. Jalil, R.M. Mhammedsharif, H. Khojasteh, S.M. Hamed, M.H. Ahmed, Comparative study of green-synthesised Ag/CuO nanocomposites: antimicrobial activity and human fibroblast cytotoxicity. Inorg. Nano-Met. Chem. (2026). https://doi.org/10.1080/24701556.2026.2640049
75. S. Tabassum, M.S. Hossain, M.A. Saeed, M.N. Uddin, S. Ahmed, Exploration of the antibacterial and photocatalytic properties of copper oxide (CuO) nanoparticles synthesized from *Azadirachta indica* leaf extract and electronic waste cable. Mater. Adv. **6**(7), 2338–2355 (2025)

Publisher's Note Springer Nature remains neutral with regard to jurisdictional claims in published maps and institutional affiliations.